Front. Earth Sci. 2016, 10(3): 578–594
DOI 10.1007/s11707-015-0536-1

RESEARCH ARTICLE

Mapping the topography and cone morphology of the Dalinor volcanic swarm in Inner Mongolia with remote sensing and DEM Data

Liwen GONG[1,2], Ni LI (✉)[1,3], Qicheng FAN[3], Yongwei ZHAO[3], Liuyi ZHANG[3], Chuanjie ZHANG[3]

1 State Key Laboratory of Earthquake Dynamics, Institute of Geology, China Earthquake Administration, Beijing 100029, China
2 Chongqing Earthquake Administration, Chongqing 401147, China
3 Key Laboratory of Active Tectonics and Volcano, Institute of Geology, China Earthquake Administration, Beijing 100029, China

Abstract The Dalinor volcanic swarm, located south of Xilinhot, Inner Mongolia of China, was a result of multistage eruptions that occurred since the Neogene period. This swarm is mainly composed of volcanic cones and lava tablelands. The objective of this study is to map the topography and morphology of this volcanic swarm. It is based on a variety of data collected from various sources, such as the digital elevation model (DEM), Landsat images, and a 1:50,000 topographic map, in addition to various software platforms, including ArcGIS, Envi4.8, Global Mapper, and Google Earth for data processing and interpretation. The results show that the overall topography of the volcanic swarm is a platform with a central swell having great undulation, sizable gradient variations, a rough surface, and small terrain relief. According to the undulating characteristics of the line profile, the volcanic swarm can be divided into four stairs with heights of 1,280 m, 1,360 m, 1,440 m, and 1,500 m. The analysis of the swath profile characterizes the two clusters of volcanoes with different height ranges and evolution. The lava tablelands and volcanic cones are distributed in nearly EW-trending belts, where tableland coverage was delineated with superposed layers of gradients and degrees of relief. According to the morphology, the volcanic cones were classified into four types: conical, composite, dome, and shield. The formation causes and classification basis for each type of volcanic cone were analyzed and their parameters were extracted. The H/D ratios of all types of volcanic cones were then statistically determined and projected to create a map of volcanic density distribution. Based on the relationship between distribution and time sequence of the formation of different volcanic cones, it can be inferred that the volcanic eruptions migrated from the margins to the center of the lava plateau. The central area was formed through superposition of multi-stage eruptive materials. In addition, a large number of early shield volcanoes were distributed on the margins. The morphological analysis of volcanic cones reveals the evolutionary stages of different types of cones. From the interpreted geomorphological indicators of faults, such as surface scarps, the pattern of volcanic cones, and the arrangement of crater major axes, it can be inferred that NE-trending and nearly EW-trending faults are present in this area, which are closely related to the formation and distribution of the volcanoes.

Keywords Dalinor volcanic swarm, volcanic geomorphology, cone morphology, cone formation and evolution, fault

1 Introduction

Volcanism directly creates and degrades landforms of the earth's surface. Thus geomorphology plays an important part in volcanic research (Thouret, 1999). In the methodology of volcanic geomorphology, Digital Elevation Model (DEM) data can be used to delineate slope gradients, altitudes, and volcanic relief (Bleacher and Greeley, 2008; Kervyn et al., 2008; Fornaciai et al., 2010). Remote sensing technologies, such as InSAR, are capable of monitoring the deformation and instability of the surface in volcanic areas (Nolesini et al., 2013) and delineating the distribution of cones and lava flow (Inbar et al., 2011). It is possible to scan cone internal structure using gravity data and aeromagnetic anomaly maps (D'Ajello Caracciolo et al., 2014; Linde et al., 2014), and gaining the magmatic activity information by geochemical data (Linde et al.,

Received January 10, 2015; accepted May 27, 2015

E-mail: lini67@sina.com

2014). The ASTER and SRIM elevation data were processed by using different software and models to obtain geologic information of volcanoes (Moon et al., 2009; Kneissl et al., 2011; Galgana et al, 2014; Gomez, 2014), thus facilitating research on mechanisms of volcanic eruptions (Thouret and Németh et al., 2012; Cashman and Sparks, 2013), the formation and evolution of volcanic landforms (Wood, 1980; Thouret, 1999; Barde-Cabusson and Merle, 2007; Delcamp et al., 2008; Prima and Yoshida, 2010; Aoki and Sidiq, 2014), and the relationship between their topographical features and hazards (Hickson et al., 2013; Huff and Owen, 2013).

The Dalinor volcanic swarm, composed of numerous volcanoes of varied sizes, is located on the Dalinor lava plateau between Xilinhot and Chifeng in the southeastern region of Inner Mongolia. It spans 115.5°−117°E, 43°−43.8°N. Studies in this area have been limited to the geochronology and petrology of, and the tectonic environment for, volcanic rock and a single volcano (the Gezishan) due to the presence of boundless grassland and traffic congestion (e.g., Yang, 1988; Luo and Chen, 1990; Liu et al., 2008; Yang et al., 2012). Note that the terrain of this area is relatively flat with single surface vegetation and little impact from human activity. It is possible to map its topography, as well as cone morphology, by using remote sensing and DEM data. Some researchers have made efforts in this direction (e.g., Li et al., 2003). However, the results from their studies seem to be inconclusive, with simple information extracted, and lacking deep analysis of the cone shape characteristics.

This study attempts to map topography and cone morphology of the Dalinor volcanic swarm using remote sensing, DEM data, and topographic maps. To process and interpret these data, we utilize various types of software, such as ArcGis9.3, Envi4.8, Global Mapper, and Google Earth. Based on the information extracted from these data, we describe the landform and cone shape of the study area in detail, and analyze the distribution, formation, and evolution of this volcanic swarm, and its relation with tectonics.

2 Tectonic setting

During the Cenozoic era, the eastern China mainland was in an extensional tectonic environment, exhibiting large-scale uplift and depression. There was a large area of basic magma eruption along the paleo-faults during the sedimentation process due to the differential vertical movement and wide variation in the composition of Mesozoic and Paleozoic faults. According to the statistics by Wu (1995), the Dalinor volcanic swarm contains 102 volcanoes in total, most of which remain intact in a cone shape. They were formed through effusion in the Pliocene–early Pleistocene. In the tectonic setting, the Dalinor volcanic swarm lies at four locations: 1) the west side of the Daxing'anling-Taihangshan gravity gradient zone, at the junction of the Xing'an and Songliao blocks, 2) the composite section of the EW-trending Tianshan-Yinshan deep faults, 3) the NE-trending Daxing'anling-Taihangshan fault, and 4) the NW-trending Abaga-Chifeng fault (Fig. 1). The volcanic rocks cover about a 3,100 km^2 area, and its lithology is mainly basalt and basanite. Abaga basalt and Beilike basalt are found northwest and Chifeng basalt southeast of this volcanic swarm. Liu et al. (2008) analyzed both major and trace elements of the rocks in this area. Their findings suggest that the basalt was formed in an extensional environment on the continental margin and intraplate, and was a result of the partial melting of mantle materials.

3 Data sources and processing

3.1 Data sources

The Dalinor volcanic swarm is characterized by a vast distribution area, with numerous volcanic cones which spread uniformly with minimal interference from other geologic bodies. This study employs elevation data and remote sensing images to extract the spatial and spectral information of the volcanic swarm.

3.1.1 Elevation data

DEM data: DEM data, e.g., the geospatial data cloud, with projection coordinates of UTM/WGS84 and spatial resolution of 30 m, were obtained from the Scientific Data Center, Computer Network Information Center, Chinese Academy of Sciences. These data were used to display the elevation undulation, the spread of lava tablelands, and the distribution of the volcanic cones for the entire volcanic swarm.

1:50,000 topographic map: This map was prepared by the Bureau of Surveying, PLA General Staff Department. The coordinate systems include the Beijing system of 1954 and the Yellow Sea elevation system of 1956, with a contour interval of 10 m and a spatial resolution of 2.5 m. The data set includes a series of topographic maps of Da'aobao, Matishan, Zhenzishan, and Keligeng. The data were mainly used for extraction of individual parameters, and analysis of the morphological characteristics of volcanic cones.

3.1.2 Remote sensing images

Landsat remote sensing data: Data were obtained from the Landsat-8 satellite launched by the National Aeronautics and Space Administration (NASA) of the USA. To enhance the display of the lava outcropping area, images acquired in April with less vegetation, a low snow

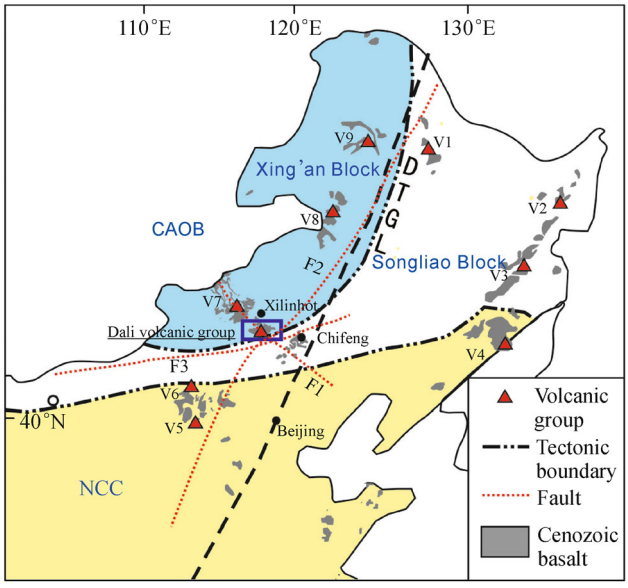

Fig. 1 Map showing tectonic setting and location (rectangular box) of the Dalinor volcanic swarm in Inner Mongolia, China (modified from Chen et al., 2013). V1: Wudalianchi volcanic group, V2: Jingpohu volcanic group, V3: Longgang volcanic group, V4: Changbaishan volcano, V5: Datong volcanic group, V6: Wulanhada volcanic group, V7: Abaga volcanic group, V8: A'ershan-Chaihe volcanic group, V9: Nuominhe-Kuilehe volcanic group, F1: Abaga-Chifeng Fault, F2: Daxing'anling-Taihangshan Fault, F3: Tianshan-Yinshan Fault, CAOB: the Central Asian Orogenic Belt, NCC: North China Craton, DTGL: Daxing'anling-Taihangshan Gravity Lineament.

coverage ratio, and low cloud content were used in this work, thus increasing the resolution of lava flows. The data covered 11 bands in total, with spatial resolutions as follows: OLI multispectral band (30 m); OLI panchromatic band (15 m); TIRS band (30 m), and a UTM-WGS84 projection coordinate system. The data were used to extract zones of lava flows and to analyze the spectral characteristics of lava.

Google Earth images: Satellite images in tiff format with a resolution of 1 m were downloaded with the Google satellite image downloader tool, and were used to improve the resolution of other bands.

3.2 Data processing

The original image data were comprised of a combination of varied and vast amounts of information. Due to the different coordinate projection systems, the image data were firstly pre-processed and enhanced to extract geographic elements. The contrast between the study area and the background was enhanced through the computation of image data, to thus extract special geomorphologic parameters.

(i) Elevation data: The elevation data included DEM data and topographic map data. The elevation data processing steps are as follows: 1) conduct pre-processing such as defining the coordinate system, image registration, image correction and cropping for the selected area, 2) generate corresponding slope gradient maps, undulation maps and washoff relief maps with the pre-processed data, and then generate contours, 3) carry out layer operation, reclassification, and weighted overlapping processing of the generated slope maps, undulation maps, and elevation maps, and 4) output map layers and prepare three-dimensional maps (Fig. 2).

(ii) Remote sensing data: In this paper, the pre-processing operations, such as image registration, correction, and cropping of multi-spectral image data were primarily conducted using the Envi4.7. The spatial resolution of the image was improved through inter-band fusion and was then enhanced through false color composite and linear stretching to highlight relevant thematic information. Finally, with the field exploration results taken into account, visual interpretation was made to extract relevant thematic information.

The specific data processing flow is shown in Fig. 2.

4 Geomorphological characteristics of volcanoes

Volcanic topographic features consist of a variety of landforms formed by volcanic activities, including those generated by volcanic cones and lava flows of different types. The Dalinor volcanic swarm is characterized by a long history of multi-stage and frequent eruptions, and diverse types of eruptions. The geomorphological characteristics of the volcanic swarm and newly formed lava

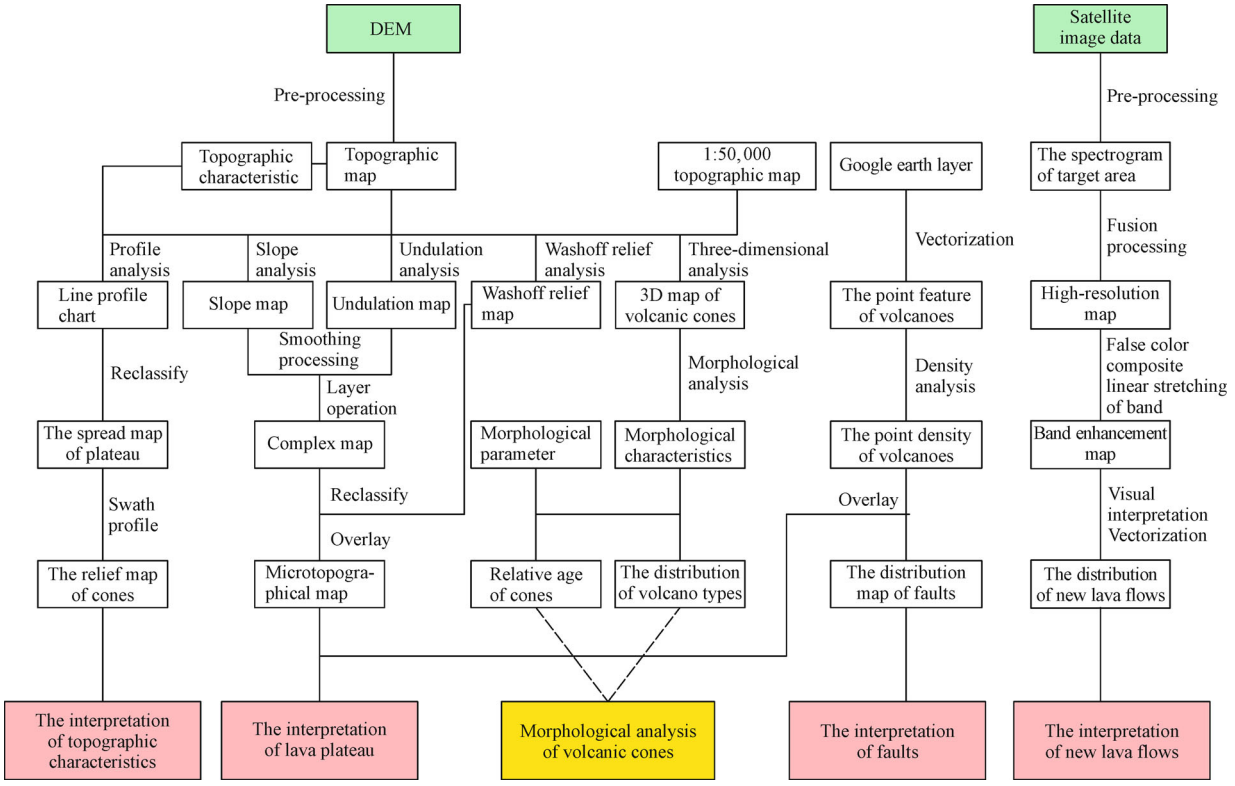

Fig. 2 Data processing flow chart.

flow boundaries were interpreted using the software ArcGIS and Envi to obtain the topographic and lava landform features.

4.1 Topographic characteristics

Overall, the Dalinor volcanic swarm exhibits a step-shaped plateau, with the central portion at a higher elevation than the margins. The surface of the plateau is relatively flat, with a raised ridge and densely distributed volcanoes. The highest point in this area is the Da'aobao volcano at an elevation of 1,694 m, and the lowest point on the margins of the plateau at 890 m. Many newly formed volcanic cones are distributed on the lava ridge in the central area of the plateau, and are roughly arranged in an EW direction. Some of these cones exhibit a beaded distribution pattern striking in the NE direction. In addition, the lava plateau extends to both the north and the south, exhibiting a compressed, thick cross shape (Fig. 3).

4.1.1 Line profile characteristics

To reveal the overall topographic undulation of the Dalinor volcanic swarm, two profile lines were drawn to traverse the lava plateau in the study area, with the crossing-point at the Da'aobao volcano. The EW-trending profile line A-B passes through more volcanic cones, with greater undulation; while the nearly NS-trending profile line C-D runs through the lava flow from north to south of the plateau, with relatively flat topography. It can be seen from the undulation of the two lines that the line A-B traverses the lava ridge with large relief and higher elevation as a whole, while the line C-D cuts the lava ridge as well as lava flows longitudinally, with large relief in the middle and gentle terrain both in the north and south sides, showing a 'convex' shape. Note that both profile lines are relatively flat at the heights of 1,280 m, 1,360 m, 1,440 m and 1,500 m, exhibiting a clear step topography (Fig. 3).

4.1.2 Swath profile characteristics

According to the undulation characteristics of transverse and longitudinal profile lines of the Dalinor volcanic swarm (Fig. 3), the DEM data of this area were classified by height (Fig. 4). As shown in Fig. 4, all stairs of the plateau exhibit a concentric spread, extending to both the east and west, with the central area at a higher elevation than the marginal areas. In addition to the dense distribution of the volcanic cones in the central areas of the plateau, a large number of volcanic cones are found in the southeastern sections, which extend to the NE with a decrease in height and undulation. As a result, the cones of the Dalinor volcanic swarm can be divided into two zones or swaths for separate research (Fig. 4).

It can be seen from Fig. 4 that the volcanic cones are densely, yet unevenly, distributed in two zones, both with

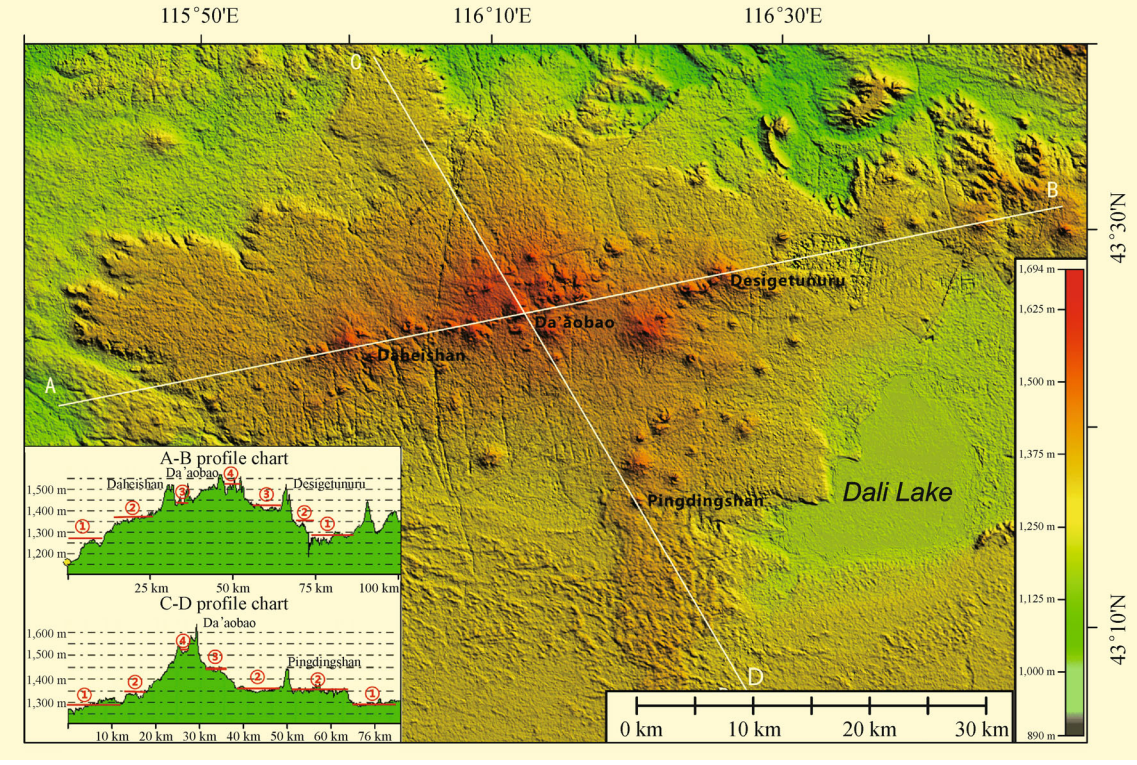

Fig. 3 Distribution characteristics of the Dalinor volcanic swarm and topographic profile lines.

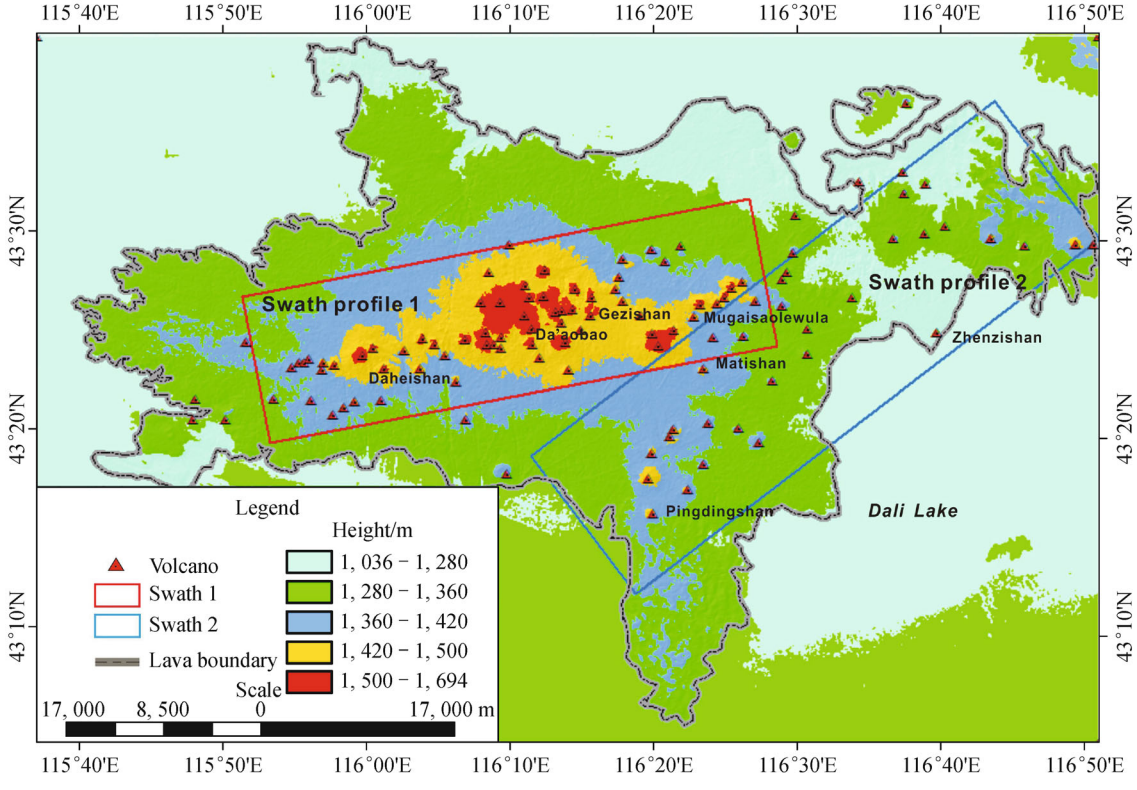

Fig. 4 DEM elevation reclassification of the Dalinor volcanic swarm. Five colors represent the topographic spread.

dominant directions. To extract the height and undulation information of the volcanic cones in both zones, a swatch profile analysis was carried out to reveal the topographic undulation within the two swaths. The elevations of cone top, cone bottom as well as the average elevation, along with their corresponding topographic reliefs in the swath ranges, are shown in Fig. 5. Their specific characteristics are as follows:

Swath 1: This swath covers most volcanoes on the central lava ridge of the plateau. There are numerous volcanoes in this zone, with distribution of the volcanic cones in an approximate EW direction. The mean elevation of this zone is about 1,400 m. The elevation variation is greater for the cone tops than that for the cone bottoms. In particular, the topographic relief in the central section with dense volcanic cones shows a zigzag shape, and typically ranges from 200 m to 250 m, whereas such reliefs at Da'aobao and Mugaisaolewula exceed 300 m (Fig. 4).

Swath 2: This swath covers most volcanoes located northeast and southeast of the plateau. The volcanic cones are relatively scattered with a specific orientation, extending in a NE direction. The average elevation of the cones is approximately 1,300 m. The elevations of cone bottoms vary around approximately 1,280 m with small amplitudes. In contrast, the elevations of cone tops change more remarkably with an amplitude about 100 m in the section with dense volcanic cones, though smaller than the relief of cone-top elevations in swath 1.

The profile lines of these two swaths indicate that the zone of swath 1 presents a high terrain with large undulation as a whole. The causes for the finally formed special geomorphology of this zone may be due to the multiple volcanic eruptions, with the eruptive materials superposed, large volumes of lava overflow, and subsequent late formation of the volcanoes. The zone of swath 2 has a low terrain and small undulation overall. The reason for this may be due to the earlier volcanic eruptions and the eruptive materials leveled over an extended period of weathering, thus causing the tendency towards a flatter terrain. Since only a few leveled volcanic cones are found

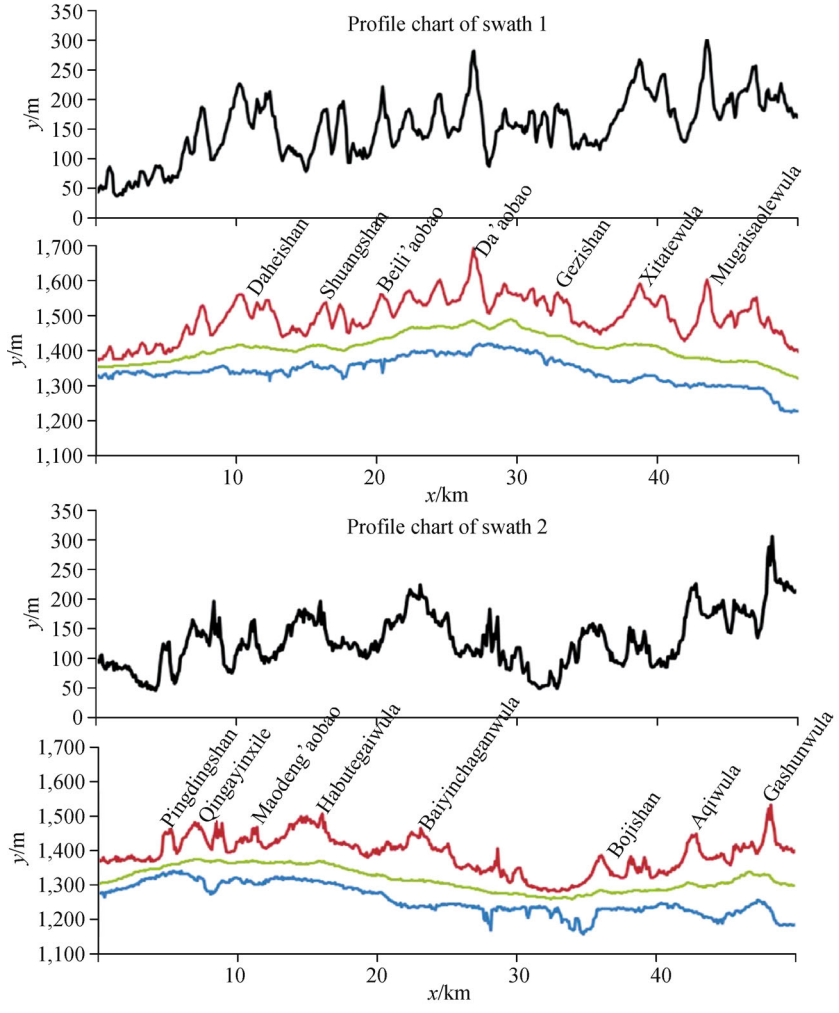

Fig. 5 Swath profiles of the Dalinor volcanic swarm showing elevations and topographic reliefs of volcanic cones. Red: elevation of cone top. Blue: elevation of cone bottom. Green: average elevation. Black: topographic relief.

northwest and southwest of the plateau, it can be inferred that the volcanic eruptions moved from the margins of the plateau to the center.

4.2 Geomorphological characteristics of lava

Lava geomorphology mainly refers to a landform formed by magma, which, after overflowing, moves on the surface, superposes onto other magma, and finally covers the surface in a flat manner. This geomorphology exhibits minimal elevation differences and gentle slopes. Due to variations in magma compositions and surface environments, different lava landforms and volcanic structures can be generated. However, since long-term weathering and denudation can level the older lava landform, which is covered by vegetation, it is difficult to directly interpret the specific landform from the elevation data. Only ravines and scarps formed from different weathering effects can be extracted by calculating the slope gradients and undulations. Therefore, the main indicators for interpretation are slope gradients and undulations, which can be used further to extract geomorphological characteristics with small elevation differences. With these two indicators, the boundaries of the lava plateau can be delineated, which in turn will determine the spread characteristics of the lava plateau. A large number of the NE-trending linear structures in the study area can also be extracted. Nevertheless, the newly formed lava flows weathered weakly, which maintained the volcanic rock structure and geomorphological characteristics. The distribution characteristics of the lava flows can also be delineated through remote sensing data interpretation.

4.2.1 Lava platform

The boundaries of the lava platform exhibit broad undulations and slope gradients. Their abnormal values are enhanced by multiplying the pixels of two map layers. In Fig. 6, the boundary of the entire lava platform is delineated, which is EW trending, with branches in north and south directions. With the resultant chart, we generated the boundary vectors of the plateau, and then calculated the spread area using the ArcGIS software, which measured approximately 2,563 km^2. In addition. Taking 1,100 m (the light green elevation in Fig. 3) as the bottom elevation of the lava plateau, and the DEM data of the plateau as the top elevation, we estimated the volume to be about 615 km^3.

4.2.2 Interpretation of newly formed lava flows

The newly formed lava flows were not completely weathered or leveled due to their late formation and brief subjection to weathering and denudation. With minimal vegetation on the surface and light colors, plus the primary structures of volcanic rock, such as fumarolic cones, fumarolic dishes, and lava ridges, that remain on the

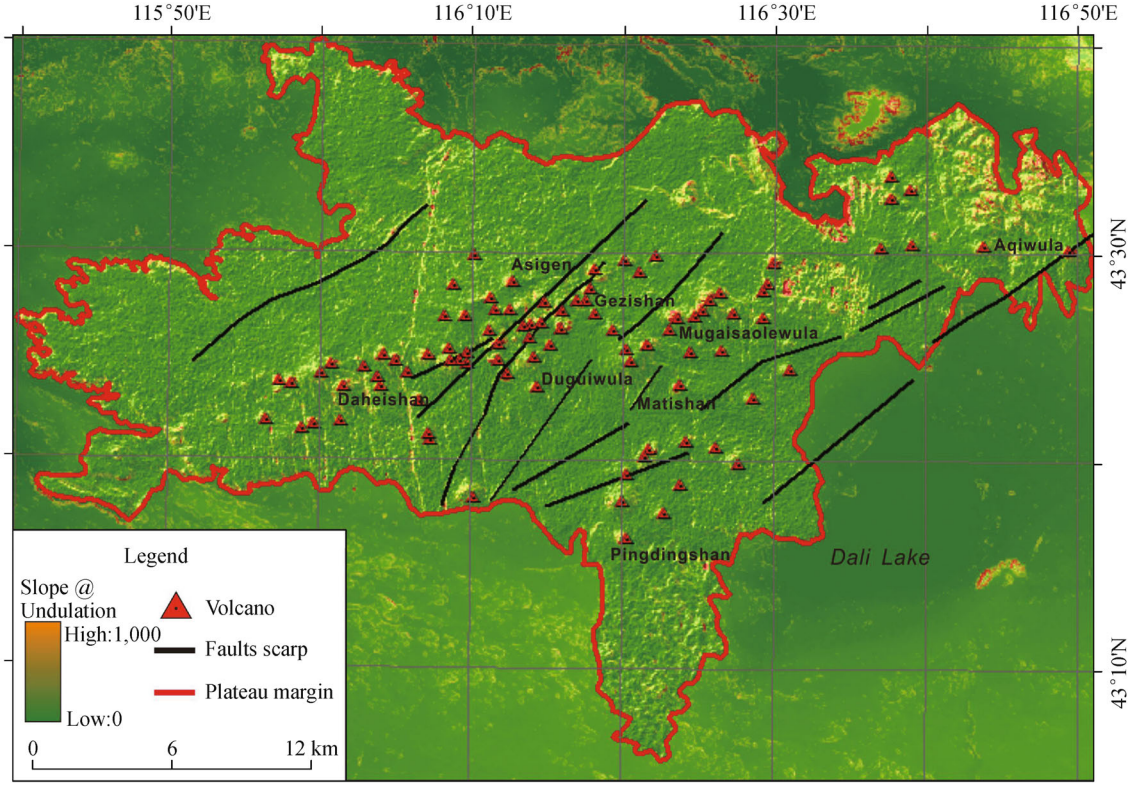

Fig. 6 Delineation of lava plateau (red line) and distribution of faults and scarps (black lines).

surface, the distribution range of the newly formed lava flows can be distinguished using remote sensing images. For the recently downloaded TM remote sensing images, we conducted pre-processing, band fusion, false color composition, and spectral linearity enhancement using the Envi software to improve the interpretation accuracy and highlighting degree of the newly formed lava flows. We also carried out artificial interpretation of these lava flows. We then verified the lava flows using Google Earth and field inspection to determine their distribution range (Fig. 7).

1) The newly formed lava flows include the Gezishan and Alatantugurige. The outcropping area of surface lava and the integrity of volcanic structures indicate that the former is younger, while the latter is older.

2) All the volcanic cones are located on the lava ridge with high terrain, and all the lava flow overflow ports are in the EW direction. However, lava flowed to the low-lying southern area, indicating that their distribution is unrelated to the direction of the overflow port, yet is greatly influenced by terrain.

3) The fluidity of the lava flows determines the similarities in thickness on the flat landform, allowing for the lava flow area to reflect the eruption volume to a certain extent. Based on ArcGIS calculations, the area of the Gezishan lava flow is 54.97 km^2, and that of the Alatantugurige is 17.04 km^2, showing that the eruption volume of the former is much larger than that of the latter.

4) The Gezishan lava overflowed from both the northeast and the west ports. Due to the existence of other volcanic cones with high terrain on either flank, lava flow was hampered. As a result, its eastern and western branches diverged to the low-lying southern area and converged there when its front edge met Wulahada and Ha'ertuolaogai. As the height of the terrain continued to increase, the lava flow was bisected further into two branches. As a whole, the lava flow shows as an "I" shape.

5) The Gezishan lava flow left behind a large number of fumarolic cones and dishes at the southern end, implying a depressed and wet swamp environment with flat terrain, which led to relatively slow lava flow movement during that time.

6) The vegetation on the Alatantugurige lava flow is flourishing with few rock outcrops, and minimal exposure on the southwestern boundary. As a result, it is difficult to further divide eruption periods.

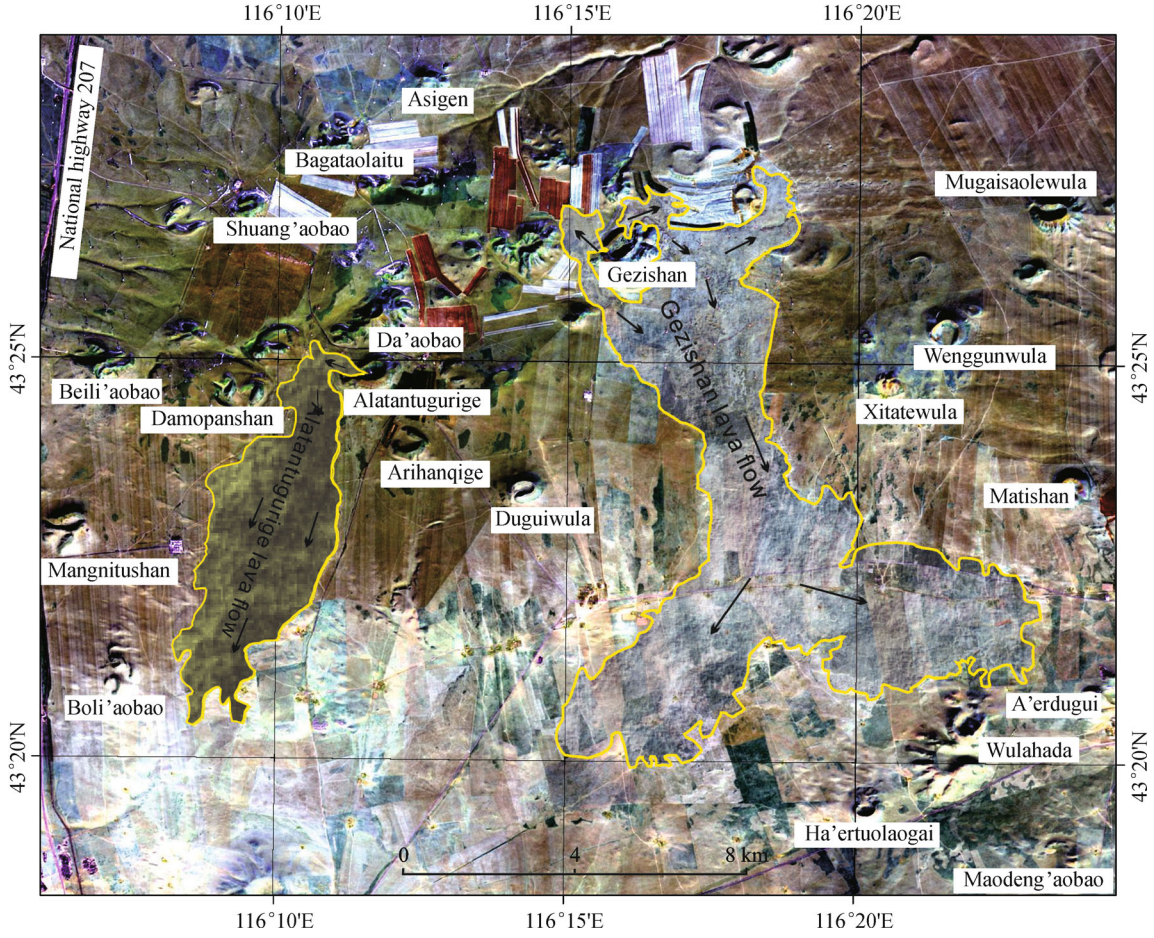

Fig. 7 Distribution of newly formed lava flows.

4.3 Morphology of volcanic cones

4.3.1 Distribution of volcanic cones

In general, volcanic cones found at considerably higher elevations, slope gradients, and undulations, characteristically have a greater variance in scale and shape than those of surrounding lava flows. As shown in Fig. 3, the volcanic cones are primarily concentrated in the central part of the platform, where cone bodies are at a relatively higher elevation and density, with significant changes in surface undulations and slope gradients, suggesting they are likely new volcanoes which were formed late. In contrast, the volcanic cones on the margins of the platform are at a relatively low elevation and are sparse, with minimal changes in undulations and slope gradients, implying they are probably old volcanoes that were formed earlier, and have been weathered and leveled over time. Thus, volcanic cones can be classified according to their morphological characteristics.

4.3.2 Morphological classification of volcanic cones

According to the morphological characteristics of the land surface, the volcanic cones in the study area can be classified into four types: conical, composite, dome, and shield; described below.

1) **Conical volcanic cone** (also called the Vesuvius type volcano) is composed of tephra or a mixture of tephra and lava, with a conical shape appearance. This type of cone is the most common in the Dalinor volcanic swarm. It exhibits a single top-truncated cone body, with a flat top, ring shape, and is typically formed with craters and lava outlets. The shapes of these craters can be circular (e.g., Matishan, Fig. 8(b)) or oval (e.g., Alatantugurige, Fig. 8 (a)). Oval craters are predominant in this area, formed with a projection of magma conduit that coincides with the major axis of corresponding oval cones. The height of the crater wall can change significantly, yet with a consistency in the direction of lava overflow ports. Only a small number of the volcanic cones exhibit a regular truncated, circular form.

2) **Composite volcanic cone** consists of a main cone and several lava overflow outlets (e.g., Da'aobao, Fig. 8(c)) or craters (e.g., Daheishan, Fig. 8(d)), exhibiting broken bodies. This cone was likely formed from continuously changing magma conduits which led to the variable crater positions. It is compounded of residual multi-stage crater walls, with incomplete crater rims and radial gullies.

3) **Dome volcanic cone** is shaped like an arch, with a gentle slope on the top, and without visible crater. Volcanic cones of this type were likely created by the accumulation of overflowing lava. Another explanation for this type of formation could be the effects of weathering and denuda-

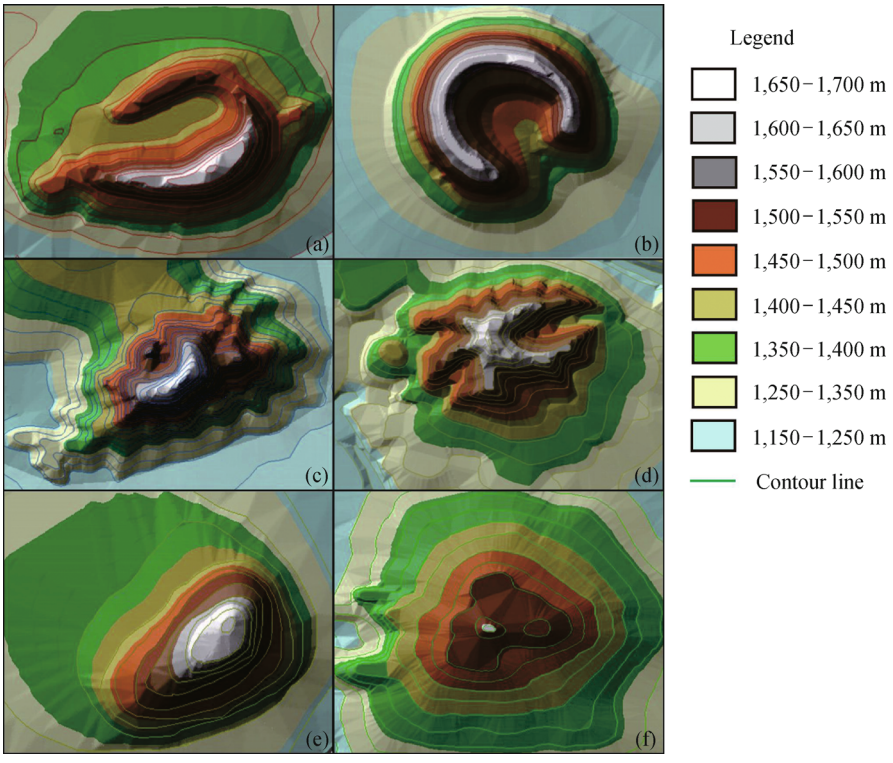

Fig. 8 3D diagrams of morphological characteristics of different volcanic cones. (a) Alatantugurige; (b) Matishan; (c) Da'aobao; (d) Daheishan; (e) Zhenzishan; (f) Qingayinxile.

tion, which caused the crater to be razed to the ground, and thus, only the root of the cone was preserved. For example, Zhenzishan (Fig. 8(e)) is a dome volcanic cone.

4) **Shield volcanic cone** was named for its gentle slope and broad and flat top. Owing to long-term weathering and leveling, its cone exhibits a gentle shield shape. The base of the cone is visibly larger, while the crater becomes smaller or even disappears. These cones were formed earlier than others, e.g., the Qingayinxile (Fig. 8(f)).

5 Parameter statistics and evolution analysis of volcanic cones

Volcanic parameters can be used to describe the scale, morphological characteristic, and size of a volcano. They can reflect to some extent the eruption direction, volume, height, and strength of a volcano. The formation age of a regularly-shaped volcanic cone can be inverted by the degree of degradation, thus permitting to infer its eruption sequence and structural control.

5.1 Parameter statistics of volcanic cones

The morphometric study of cinder cones has proven to be an efficient tool for determining their eruption episodes and erosion processes (Inbar and Risso, 2001; Parrot, 2007). The measurements and calculations of the Dalinor volcanic swarm cone parameters (Table 1) made in this work were based on a combination of field geological investigations, and the 1:50,000 topographic map and satellite images downloaded from Google Earth. The statistics show that there are a total of 102 volcanic cones in the Dalinor volcanic swarm, including 14 composite volcanoes, 50 conical volcanoes, 28 dome volcanoes, and 10 shield volcanoes (Table 1, only named volcanoes shown in the 1:50,000 topographic map are listed). Owing to the irregular shapes of volcanic cones in this area, this work used the highest elevation and the maximum undulation difference of each cone to facilitate the statistics. The diameters of the cones with oval bottoms were measured by using both the minor and the major axes. The ratio of cone height to diameter (H/D) was obtained by subtracting the cone bottom diameter from the crater diameter, which can reflect the formation time of a cone to a certain extent. The direction of lava overflow outlet is that of the residual gap of the volcanic cone.

5.2 Evolutionary processes of volcanic cones

A volcanic cone experiences various evolutionary processes after its formation, such as weathering, denudation, transportation, and accumulation, and is then eroded into a low and flat dome-like volcano. Wei et al. (2003) considered that there is a positive correlation between the diameter of the cone bottom and the depth of the crater pit. They also stated that the low and flat craters formed during an earlier stage can be clearly distinguished from the volcanic cones formed during a later stage according to the difference observed between the cone bottom and crater rim diameters, and the height of the volcanic cone. Inbar et al. (2011) thought that the measurement of morphology of a volcanic cone is the most effective tool to determine the relative age of a volcano. Taking the Tolbachik volcanic area as an example, they studied the relationship between the cone height/width ratio, the volcanic erosion rate, and relative age. The results show that the erosion rate of a volcanic cone has some regularity; that is, the height of a cone, the diameter of a crater, the depth of a crater pit, and the slope gradient of a cone's outer surface decrease over time, while the width of the crater wall rim and the diameter of the cone bottom consistently increase. The increase rate of the diameter of the cone bottom is much greater than that of the diameter of the cone top; namely, the difference between the diameter of the cone bottom and the width of the crater wall rim also continually increase with the passage of time. Thus, the evolutionary process of a volcanic cone can be indicated in terms of the height of a cone, the diameter of a cone bottom, the crater rim, and the slope gradient of a cone. Due to the significant slope gradient variances at different cone positions, certain measurement errors will be made. For those volcanic cones with a regular circular shape, there is a relationship between the average slope gradient of a volcano (S), the height of the cone (H), the diameter of the cone bottom (D_o), and the diameter of the crater rim (D_i) as follows:

$$S = \arctan\left(2H/(D_o - D_i)\right). \quad (1)$$

Eq. (1) shows that the cone slope gradient can be replaced by the ratio of the height of the cone to the diameter of the cone. Therefore, to simplify the calculation, we used the value of H/D to indicate the evolutionary degree of a cone.

Using the statistics of H/D values of various cones in Table 1, a histogram (Fig. 9) was plotted using average values. It is clear that the H/D values are related to properties of the cones and change significantly with cone types. Overall, there are significant differences in H/D values of the four cone types, which are in a descending order of magnitude: conical, dome, composite, and shield. Eq. (1) also indicates that the H/D value is positively proportional to the slope gradient S, which is an important reference variable for identifying the cone age. That is to say, the greater the cone slope gradient, the younger the age, i.e., the younger the cone. Thus the evolutionary process of a cone from new to old can be considered as: conical → dome → shield (a composite volcano is compounded by volcanoes of multiple eruption episodes, so its H/D value cannot reflect its evolutionary sequence).

Table 1 Parameter statistics of Dalinor volcanic cones

Cone type	Volcano name	Latitude	Longitude	Altitude/m	Height /m	D_co /m	D_cr /m	*H/D*	DLOP
Conical cones	Manituwula	43.42°N	116.06°E	1,551	91	844/1,325	389/694	0.167	NNW
	Shuang'aobao	43.45°N	116.16°E	1,624	84	743/971	230/442	0.161	NW
	Bagataolaitu	43.46°N	116.19°E	1,568	68	789/897	424/603	0.206	NNW
	Bojishan	43.55°N	116.65°E	1,371	101	1,130	690	0.230	N
	Gasongshan	43.50°N	116.82°E	1,561	131	990	350	0.205	WN
	Niujuanshan	43.50°N	116.86°E	1,390	48	780	390	0.123	E
	Haoraoertaolaigai	43.36°N	115.99°E	1,476	76	760	390	0.205	NE\W
	Benghenwula	4.335°N	115.85°E	1,377	67	1,150	460	0.97	NE
	Zhazhigayinwula	43.36°N	115.90°E	1,412	52	1,050	602	0.117	
	Xilinyinha-butewula	43.36°N	115.94°E	1,431	51	1,030	440	0.086	WN
	Achabayanwula	43.49°N	116.50°E	1,443	103	1,270	830	0.234	W/NE
	Alatantugurige	43.41°N	116.19°E	1,601	101	851/1,230	448/695	0.215	NWW
	A'rihanqige	43.40°N	116.21°E	1,513	63	755/925	386/580	0.176	NW
	Douguiwula	43.39°N	116.24°E	1,525	85	911/1,043	333/571	0.162	W
	A'ergengqige	43.44°N	116.26°E	1,601	111	966/1,472	510/944	0.226	NWW NNE
	Gezishan	43.45°N	116.26°E	1,568	68	614/694	329/396	0.233	NNE
	Jiaxianzi	43.42°N	116.34°E	1,572	42	391/441	160/227	0.189	NNW
	Megaxiarong	43.44°N	116.38°E	1,489	69	571/855	332/498	0.231	W
	Mugaisaolewula	43.45°N	116.39°E	1,609	119	953/1,355	397/687	0.194	NW
	Bagasuorong	43.46°N	116.44°E	1,502	92	780/1,036	366/468	0.187	NW
	Sifangshan	43.45°N	116.45°E	1,458	48	537/774	280/554	0.201	W
	Desigetunuru(a)	43.46°N	116.43°E	1,581	101	946/1,345	509/746	0.195	NW
	Desigetunuru(b)	43.45°N	116.42°E	1,521	71	751/1,046	367/702	0.195	NE SWW
	Desigetunuru(c)	43.45°N	116.41°E	1,524	54	721/784	477/489	0.206	NW
	Wulahada	43.34°N	116.36°E	1,489	89	1,165/983	575/618	0.198	NE
	Aobordouguiwula	43.34°N	116.44°E	1,402	52	659/937	465/612	0.200	SWW
	Mangnitushan	43.38°N	116.11°E	1,464	64	750/1,176	416/740	0.166	NW
	Matishan	43.39°N	116.39°E	1,523	103	938	468	0.219	SE
	Pingdingshan	43.27°N	116.34°E	1,470	80	1,400	618	0.102	
	Wenggunwula	43.43°N	116.36°E	1,592	82	1,000	632	0.223	SSE
	Sumi'aobao	43.29°N	116.38°E	1,496	96	966	347	0.155	NW
	Ha'ertuolaogai	43.32°N	116.34°E	1,487	87	897	500	0.219	NNW
	Baiyinchaganwula	43.40°N	116.51°E	1,404	74	889	407	0.154	NW
Composite cones	Da'aobao	43.43°N	116.20°E	1,699.6	202	1,198/2,140	238/370	0.148	NW
	Asigen	43.43°N	116.20°E	1,621	121	952		0.127	
	Boli'aobao	43.35°N	116.12°E	1,412	53	975		0.054	
	Beili'aobao	43.42°N	116.12°E	1,582	82	824/1,320		0.076	
	Wu'aobao	43.41°N	116.01°E	1,553	103	576/1,243		0.113	
	Daheishan	43.39°N	116.03°E	1,565	125	822/1,683		0.100	
	Shejigengang	43.49°N	116.30°E	1,485	65	980/1,604		0.050	
	Xitatewula	43.41°N	116.34°E	1,612	82	902/1,631		0.065	

(*Continued*)

Cone type	Volcano name	Latitude	Longitude	Altitude/m	Height /m	D_co /m	D_cr /m	*H/D*	DLOP
	Ya'ergaitewula	43.39°N	115.97°E	1,459	97	1,280		0.076	
	Aqiwula	43.50°N	116.73°E	1,491	121	1,040		0.116	
Dome cones	Shuangshan	43.39°N	116.07°E	1,502	72	772/902		0.086	
	Zhenzishan	43.43°N	116.67°E	1,347	57	206/307		0.222	
	Jiazishan	43.45°N	116.49°E	1,430	50	965/711	393	0.092	
	Langwoshan	43.45°N	116.57°E	1,364	54	628/938	469	0.098	
	Achahai'erhan	43.50°N	116.77°E	1,394	54	330		0.164	
	Talinhua	43.41°N	115.87°E	1,395	55	670		0.086	
	Chulute	43.39°N	115.92°E	1,426	46	430		0.106	
	Duo'erbole-jinxire	43.34°N	115.80°E	1,343	53	450		0.118	
	Erduntaolegai	43.56°N	116.63°E	1,359	79	690		0.114	
Shield cones	Damopanshan	43.41°N	116.14°E	1,587	87	2,000		0.044	
	Ha'er'aobao	43.41°N	116.34°E	1,612	67	958		0.059	
	A'erdougui	43.35°N	116.40°E	1,439	49	713		0.054	
	Maodeng'aobao	43.31°N	116.40°E	1,419	59	948		0.052	
	Qingayinxile	43.30°N	116.33°E	1,479	89	2,893		0.027	
	Habutegaiwula	43.33°N	116.46°E	1,398	48	2,082		0.023	
	Huitengxile	43.35°N	115.97°E	1,429	39	1,200		0.036	

Note: In this table, only named volcanoes in the 1:50,000 topographic map are listed. Abbreviations: D-co: Diameter of cone, D-cr: Diameter of crater, DLOP: Direction of lava overflow port.

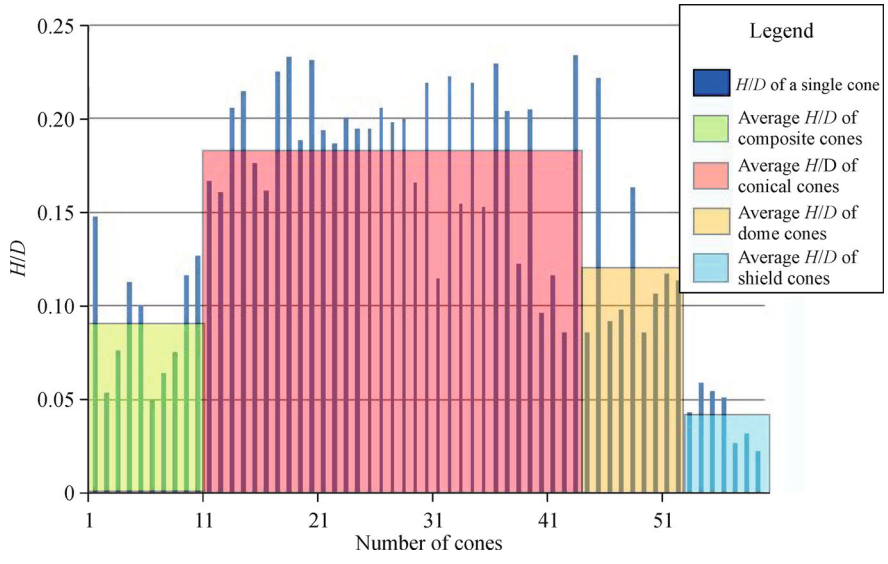

Fig. 9 *H/D* values of cones with different morphological characteristics in the study area.

5.3 Age estimation of volcanic rock

According to the 1:200,000 regional survey information offered by the Inner Mongolia Geological Bureau, all the basalts are intercalated in the Quaternary Pleistocene sand mud beds. The first layer of basalt exhibits disconformity on the Pliocene brick-red mudstone, and its time of formation was thought to be the Pleistocene. Luo and Chen (1990) have obtained the K-Ar ages of basalt from boreholes in Dalinor-Changtu'aobao and Huitengxili, which are 1.18 Ma and 1.45 Ma, respectively. The K-Ar age of basalt from the Xilinhot reservoir is 0.47 Ma, and that of the cone lava in the A'ergengqige volcano (Gezishan) is 0.33 Ma. Chen et al. (2013) performed K-

Ar dating for Beilike basalt (adjacent to the north of the Dalinor volcanic swarm), resulting from the Middle Pleistocene to the Late Pliocene (0.51–2.41 Ma). Therefore, previous studies divided the volcanic eruption period into at least three epochs, namely the early Miocene (15.42 Ma), the late Pliocene (about 3.21 Ma), and the Pleistocene (1.18–0.33 Ma). These volcanoes have been leveled by long-term weathering and denudation. No volcanic cone of these ages is currently present on the ground surface.

Based on the evolutionary law of volcanic cones, if dot projection is conducted for the ratio of the diameter to the height of a cone, one can distinguish the cones of different ages. Based on the degradation law of volcanic cones and existing dating data, Hooper and Sheridan (1998) obtained the relationship between the H/D value of cones and volcanic eruption age Y by statistics:

$$H/D = 0.266\exp(-1.213Y). \quad (2)$$

Namely,

$$Y = \frac{-\ln\left(\frac{H/D}{0.266}\right)}{1.213}. \quad (3)$$

This work used the empirical Eq. (3) to calculate the relative eruption ages of cones to give a rough judgment of the relative time sequence for the volcanic cones. Here the H/D value of each volcanic cone is substituted into the equation to achieve a corresponding age. The calculated results are as follows: the newest eruption age (Gezishan) is 0.136 Ma and the oldest (Habutegaiwula) is 2.02 Ma. The average age of conical volcanoes is 0.31 Ma, whereas that of dome and shield volcanoes are 0.65 Ma and 1.53 Ma, respectively, consistent with dating results obtained by other researchers. ArcGIS software was then used to mark the relative age of each cone onto the corresponding cone with histogram, and to denote different cone types with different symbols and colors (Fig. 10). It can be seen that the volcanoes in the middle of the lava ridge are of higher density, with multifarious cone types and substantial change in relative ages, indicating a greater time span of volcanism in this area. In addition, this is a primary distribution area of composite volcanoes, suggesting that it experienced many episodes and times of volcanism and that the volcanic morphology was the combined result of multi-stage volcanism. In contrast, the volcanoes close to the northwestern shore of Lake Dalinor exhibit low cone density and simple morphological cone characteristics, and are dominated by both shield volcanoes and gentle conical volcanoes without composite volcanoes, implying that the volcanism was relatively weak and occurred earlier, with few episodes and times in this area.

6 Formation model of conical volcanoes

Statistics show that most of the cones in the Dalinor volcanic swarm are of conical shape, with differences in top heights. The crater walls on the southeast side are 20–70 m higher than those on the northwest side. Such differences gradually diminish with growing cone denudation. In addition, the lava overflow outlets of these volcanoes trend in the NNW to W directions, just to the lower side of the crater rim. The northeastern and southwestern portions of the cones are relatively weak,

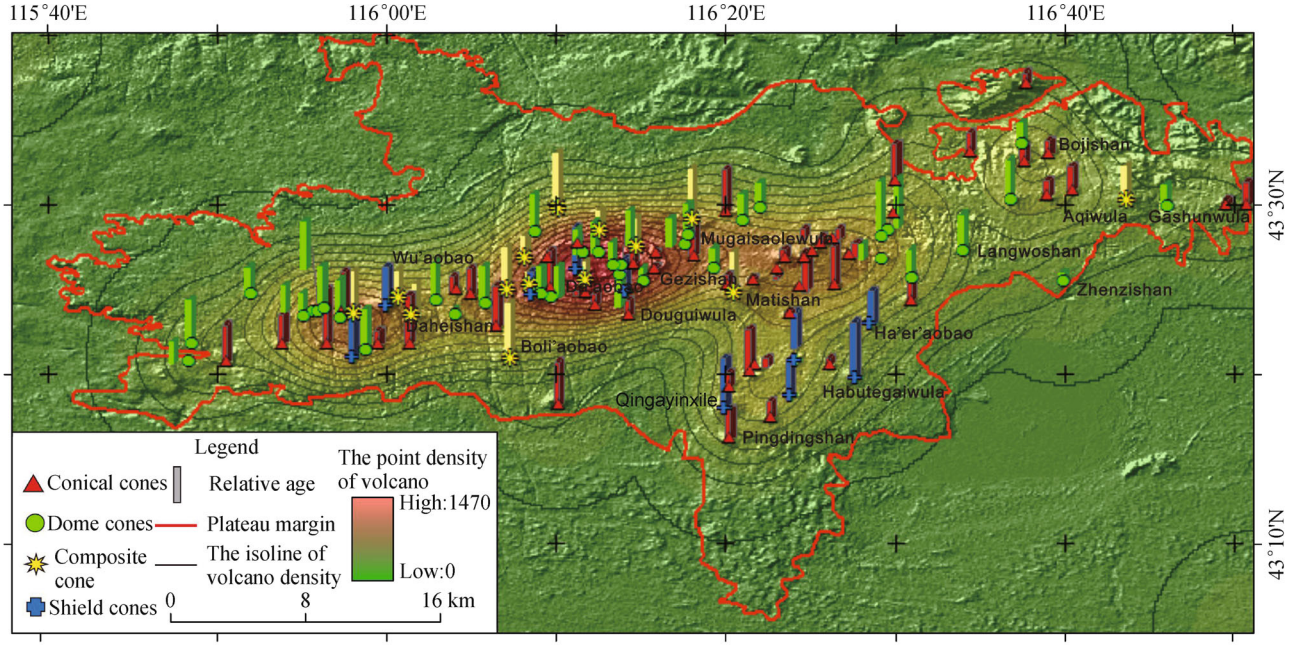

Fig. 10 Distribution of various types of volcanic cones and their relative ages in the study area.

and likely serve as dominant outlets for lava overflow. Hence, the formation model of the cones can be established by inverting the existing morphological characteristics of the cones.

The morphological characteristics of the cones show that the volcanic accumulation on the southeast side of the Mugaisaolewula cone is obviously more than that on the northwest side. In addition, the crater wall on the southeast side is also higher than that on the northwest (Fig. 11). The Matishan cone shows a regular truncated conical shape, on which eruption products are uniformly distributed (Fig. 8 (b)). Both the cones were formed on flat tableland, with less influence from the surrounding terrain. Two possible factors can result in uneven distribution of volcanic accumulations: dragging of lava flow and tilting of magma conduits.

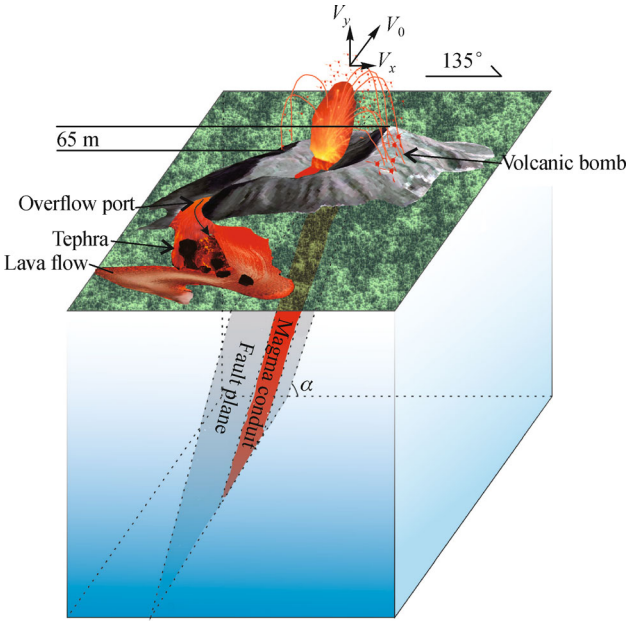

Fig. 11 Formation model of a truncated elliptic cone.

1) Dragging lava flow: According to the statistics, most lava overflow outlets face NNW to W. These lava flows drag a large amount of tephra from the cones, decreasing volcanic debris northwest of the cone, thus creating a lower crater wall.

2) Tilting of magma conduits: The weak fault plane was the main magma conduit during magma ascent. If the basement faults tilt toward the northwest, the magma conduit mouths face toward the southeast. Thus the volcanic tephra had a component velocity (V_x) in the SE direction along the fault dip during the process of eruption. In particular, the volcanic bombs and xenoliths were less influenced by the environment, most of which fell on the southeast side of the cone with minimal amounts of small or fine volcanic tephra scattered on the northwest side. Field investigations also found a large number of volcanic bombs and mantle xenoliths on the southeastern slope of the cone. Other NE-trending volcanoes in beaded distribution share similar features. These phenomena demonstrate that the main factor influencing the formation of volcanic cones with such characteristics is the tilting of magma conduits.

7 Interpretation of fault distribution characteristics

7.1 Tectonic setting

As stated earlier, the Dalinor volcanic swarm lies at the conjunction of the deep EW-trending Tianshan-Yinshan fault and the NE-trending Daxing'anling-Taihangshan fault, roughly concentrated along the NEE trend. Li and Ouyang (1998) argued that this region is situated in the collage composed of multiple small blocks west of the Xing'an-Mongolian orogenic belt, where the tectonic pattern and evolution have been changing steadily, creating the conditions for Cenozoic magmatic activity. Luo and Chen (1990) have studied the tectonic setting of this area in detail. They suggest that the Inner Mongolia basalt area had been located on the western side of the North China rift system since the Cenozoic and that the basic volcanic activity moved from the center of the rift system to either side, taking the deep faults as magma conduits since the Neogene.

7.2 Fault signs

Previous studies found that the distribution of volcanoes, the extension of lava flows, and geomorphic features of volcanoes are largely influenced by faults (Jiang et al., 2003; Wang and Chen, 2005). These findings provide a new line of thought for the interpretation of faults. We can identify the fault distribution and extension direction according to the fault marks, including tectonic signs and geomorphological features. As shown in the 1:200,000 Xilinhot geological map, there are multiple NEE- and NE-trending faults in the Carboniferous and Jurassic strata outcropping north of the lava platform, and EW-trending faults appear in the Permian strata exposed east of the platform. Due to coverage of lava flows, there is no obvious tectonic mark in the central area of the platform. Nevertheless, numerous geomorphological signs, such as fault scarps, volcanoes of beaded distribution, and the alignment of volcanic cones, indicate the presence of possible NE-trending faults in this area.

7.2.1 Fault scarps

Due to the small differences in the elevation of fault scarps

in this area, it is difficult to distinguish them using original elevation data. Alternatively, geomorphological anomalies can be extracted by calculating slope gradients and undulations using interpretation of remote sensing data. As shown in Fig. 6, there are over ten linear elements arranged in the nearly NE trend on the lava platform, some of which pass through volcanoes, some are parallel to volcanoes, and still others are located on the extension lines of the volcanic alignment. These lines of evidence indicate that basement faults could possibly be hidden beneath the Dalinor volcanic swarm, and thus controlled the distribution and eruption of the volcanoes.

7.2.2 Volcanic distribution

As mentioned above, numerous volcanoes are situated on the lava platform in this area, with regularity in distribution. Most volcanic cones are of a linear or beaded distribution, particularly the NE-trending beaded Xitatewula-Mugaisaolewula-Bagasuorong, showing a strong consistency between volcanic morphological characteristics and eruption types (Fig. 12(a)). This work calculated volcanic density using coordinates of volcanoes. The resultant map shows that two dominant volcanic distribution directions, NE and NEE (Fig. 12(b)), and the degradation degree of the volcanic cones are closely related to such volcanic distribution, which coincides with the dominant strikes of regional faults. Thus we suggest that the faults in this area, most likely the extensional faults, may be the conduits of magma ascent, thus controlling volcanic distribution.

7.2.3 Major axis trends of volcanic cones

More than half the cones of the Dalinor volcanic swarm exhibit the truncated elliptic form, and the major crater axes are of similar orientations. However, due to the variance in eruption times or eruption types of the cones, many have lost their craters. Therefore, we attempted to find evidence of basement faults by using the statistics of the major axis directions of the volcanic cone bottoms. The specific method is as follows: Extract the polygons of cone bottoms using the high-accuracy data from Google Earth, and then conduct vector transformation. The major axis directions of the irregular polygons are subsequently extracted using the Envi software, and statistics ais carried out by using Excel to create a radar chart (Fig. 13). The results show that the major axes of approximately 90% of the volcanic cones in the volcanic swarm fall within 50°–70°, implying in the nearly NEE trend, consistent with other fault marks.

In sum, from overall spread of the volcanic swarm, linear geomorphology, beaded distribution of cones, and dominant direction of major axes of cone bottoms, in conjunction with geological maps and previous studies, we infer that there exist NE and nearly EW trending faults beneath the lava platform of the study area. On a larger scale, the volcanic swarm was likely associated with the joint effects of the EW-trending Tianshan-Yinshan fault and the NE-trending Daxing'anling-Taihangshan fault.

8 Conclusions

The Dalinor volcanic swarm resulted from the occurrence of multistage eruptions since the Neogene period. This swarm is mainly composed of volcanic cones and lava tablelands. In this study, based on the DEM data and remote sensing images, some geomorphological elements were extracted using image processing software such as ArcGIS9.3 and Envi4.8. Coupled with the relationships between these elements, we have analyzed the genesis, classification, and time sequence relationships of the volcanic cones, as well as the influence of the faults on the volcanic cones. The conclusions of this work are stated below.

1) Geomorphology of lava plateau: The boundary of the lava platform was highlighted by multiplying the slope

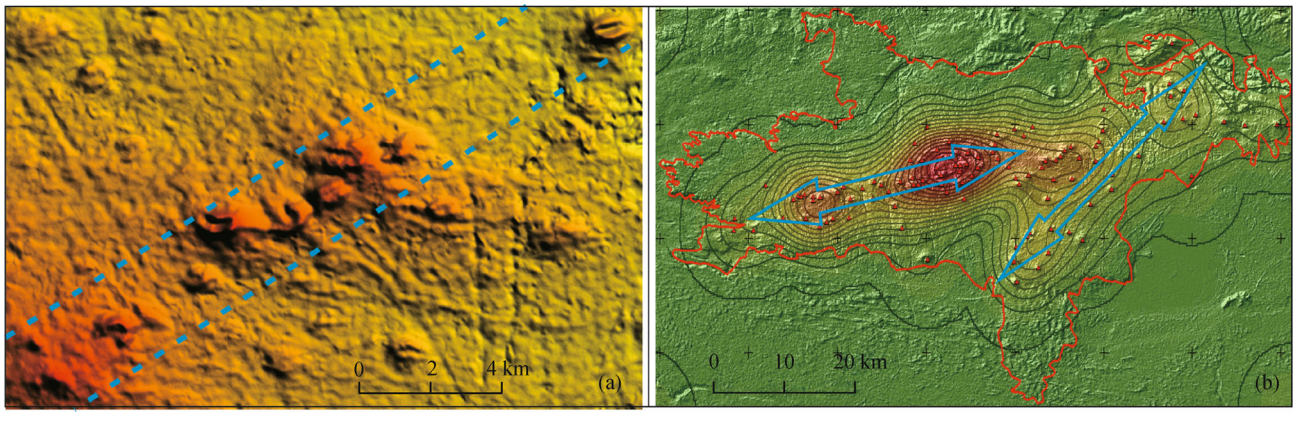

Fig. 12 Beaded distribution of volcanoes (a) and volcano distribution density (b).

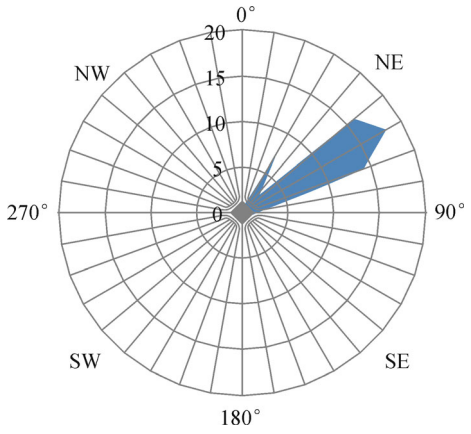

Fig. 13 Statistical graph of major axes of cone bottoms in the study area.

gradient with the undulation, so as to delineate the range of the lava platform. This lava platform spreads as an EW-trending belt, with small branches in both south and north directions. Using ArcGIS, the area and volume of the lava plateau were estimated to be about 2,563 km^2 and 615 km^3, respectively.

2) Geomorphology of newly formed lava flows: With such means as band selection based on the Envi software, band information enhancement, and visual interpretation, we extracted the boundary of newly formed lava flows, and determined the direction of their overall flow to be toward the low-lying south. The lava flow areas of Gezishan and Alatantugurige are 54.97 km^2 and 17.04 km^2, respectively, showing the eruption volume of the former to be much larger than that of the latter. According to the locations of fumarolic cones and fumarolic dishes, it was inferred that the southern sections of the lava flows were in a wet swamp environment.

3) Geomorphology of volcanic cones: The volcanic swarm was graded by elevations based on the line profiles. In addition, two swath profiles were used to analyze the overall distribution characteristics of the volcanic cones in the two clusters. With the help of 3D visualization diagrams, the volcanoes were classified into four types according to the morphological characteristics of the volcanic cones: composite, conical, dome, and shield. By using the statistics of the morphological parameters of the different types of cones and then projecting them on a map, an evolution model of the volcanic swarm was constructed as follows: In its early stage of formation, the swarm contained large amounts of magma, and the volcanoes were widely distributed over the entire platform. In the later stages, the magma volume decreased and the volcanoes were primarily concentrated in the central area of the platform. The high terrain of this area was produced by superposition of multiple episodes of volcanic eruptions.

4) Analysis of volcanic cone morphology: Lava overflow outlets were controlled by structures, and lava flow directions were determined by terrain. In combination with the results of previous studies, this work has also revealed the relative age characteristics of different volcanic cones, and indicated their evolutionary degree. Combined with the morphological characteristics of the cones in this area, this study has established the formation model and evolutionary process of the conical volcanoes.

5) Hidden faults: Interpretation of remote sensing data in terms of the ArcGis 9.3 and Envi 4.8 software reveals the overall spatial pattern of the Dalinor volcanic swarm, in addition to its geomorphological linear elements, beaded distribution, and major axis azimuths of volcanoes. We thus infer that there exist NE-trending and nearly EW-trending faults in the basement of the lava platform in this area. In combination with the 1:200,000 geological map and previous work, we suggest that the overall distribution of this volcanic swarm is likely associated with the joint effect of the EW-trending Tianshan-Yinshan fault and the NE-trending Daxing'anling-Taihangshan fault.

Acknowledgements This work was supported by the program "Volcanic rock chronology of the Xilinhot volcanic swarm in Inner Mongolia" funded by the National Key Laboratory of Earthquake Dynamics, Institute of Geology, China Earthquake Administration (LED2013B05) and the program "Genesis and evolution of the Quaternary Dalinor volcanic swarm" funded by the National Natural Science Foundation of China (Grant No. 41572320).

References

Aoki Y, Sidiq T P (2014). Ground deformation associated with the eruption of Lumpur Sidoarjo mud volcano, east Java, Indonesia. J Volcanol Geotherm Res, 278–279: 96–102

Barde-Cabusson S, Merle O (2007). From steep-slope volcano to flat caldera floor. Geophys Res Lett, 34: 1–5

Bleacher J E, Greeley R (2008). Relating volcano morphometry to the developmental progression of Hawaiian shield volcanoes through slope and hypsometric analyses of SRTM data. J Geophys Res, 113: 1–8

Cashman K V, Sparks R S J (2013). How volcanoes work: a 25 year perspective. Geol Soc Am Bull, doi: 10.1130/B30720.1

Chen S S, Fan Q C, Zhao Y W, Shi R D (2013). Geochemical characteristics of basalts in Beilike area and its geological significance, Inner Mongolia. Acta Petrologica Sinica, 29(8): 2695–2708 (in Chinese)

D'Ajello Caracciolo F, Nicolosi I, Carluccio R, Chiappini S, De Ritis R, Giuntini A, Materni V, Messina A, Chiappini M (2014). High resolution aeromagnetic anomaly map of Mount Etna volcano, Southern Italy. J Volcanol Geotherm Res, 277: 36–40

Delcamp A, van Wyk de Vries B, James M R (2008). The influence of edifice slope and substrata on volcano spreading. J Volcanol Geotherm Res, 177(4): 925–943

Fornaciai A, Bisson M, Landi P, Mazzarini F, Pareschi M T (2010). A LiDAR survey of Stromboli volcano (Italy): digital elevation model-

based geomorphology and intensity analysis. Int J Remote Sens, 31 (12): 3177–3194

Galgana G A, Newman A V, Hamburger M W, Solidum R U (2014). Geodetic observations and modeling of time-varying deformation at Taal Volcano, Philippines. J Volcanol Geotherm Res, 271: 11–23

Gomez C (2014). Digital photogrammetry and GIS-based analysis of the bio-geomorphological evolution of Sakurajima Volcano, diachronic analysis from 1947 to 2006. J Volcanol Geotherm Res, 280: 1–13

Hickson C, Spurgeon T, Tilling R, Adam P (2013). Factors influencing volcanic hazards and the morphology of volcanic landforms. In: Shroder J, James L A, Harden C P, Clague J J, eds. Treatise on Geomorphology. San Diego: Academic Press, 219–242

Hooper D M, Sheridan M F (1998). Computer-simulation models of scoria cone degradation. J Volcanol Geotherm Res, 83(3–4): 241–267

Huff W D, Owen L A (2013). Volcanic landforms and hazards. In: Shroder J, James L A, Harden C P, Clague J J, eds. Treatise on Geomorphology, San Diego: Academic Press, 148–192

Inbar M, Gilichinsky M, Melekestsev I, Melnikov D, Zaretskaya N (2011). Morphometric and morphological development of Holocene cinder cones: a field and remote sensing study in the Tolbachik volcanic field, Kamchatka. J Volcanol Geotherm Res, 201(1–4): 301–311

Inbar M, Risso C (2001). A morphological and morphometric analysis of a high density cinder cone volcanic field-Payun Matru, south-central Andes, Argentina. Z Geomorphol, 45: 321–343

Jiang C S, Zhou R Q, Zhao C P (2003). The relationship between the tectonic geomorphic features and volcano activity in Tengchong regeion. Journal of Seismological Research, 26(4): 361–366 (in Chinese)

Kervyn M, Ernst G G J, Goossens R, Jacobs P (2008). Mapping volcano topography with remote sensing: ASTER vs. SRTM. Int J Remote Sens, 29(22): 6515–6538

Kneissl T, van Gasselt S, Neukum G (2011). Map-projection-independent crater size-frequency determination in Gis environments——New software tool for ArcGis. Planet Space Sci, 59(11–12): 1243–1254

Li F T, Chu Y, Zhong W C (2003). New remote sensing interpretation of volcanic groups in Gankui and Nuomin-Bilahe, Inner Mongolia. Remote Sensing for Land & Resources, 54(3): 20–24 (in Chinese)

Li S L, Ouyang Z Y (1998). Tectonic framework and evolution of Xing Anling-Mongolian orogenic belt (XMOB) and its adjacent region. Marine Geology & Quaternary Geology, 18(3): 45–54 (in Chinese)

Linde N, Baron L, Ricci T, Finizola A, Revil A, Muccini F, Cocchi L, Carmisciano C (2014). 3-D density structure and geological evolution of Stromboli volcano(Aeolian Islands, Italy) inferred from land-based and sea-surface gravity data. J Volcanol Geotherm Res, 273: 58–69

Liu J J, Zhang Y Q, Zhao J F (2008). The characteristic of the cenozoic basalt and its formed tectonic setting in the Ximeng, Inner Mongolia. Theory Deliberated, 5: 56–58 (in Chinese)

Luo X Q, Chen Q T (1990). Preliminary study on geochronology for Cenozoic basalts from Inner Mongolia. Acta Petrological Et Mineralogica, 9(1): 37–49 (in Chinese)

Moon V, Bradshaw J, de Lange W (2009). Geomorphic development of White Island Volcano based on slope stability modelling. Eng Geol, 104(1−2): 16–30

Nolesini T, Di Traglia F, Del Ventisette C, Moretti S, Casagli N (2013). Deformations and slope instability on Stromboli volcano: integration of GBInSAR data and analog modeling. Geomorphology, 180–181: 242–254

Parrot J F (2007). Tri-dimensional paramerization: an automated treatment to study the evolution of volcanic cones. Geomorphology, 3: 247–257

Prima O D A, Yoshida T (2010). Characterization of volcanic geomorphology and geology by slope and topographic openness. Geomorphology, 118(1−2): 22–32

Thouret J C (1999). Volcanic geomorphology—An overview. Earth Sci Rev, 47(1–2): 95–131

Thouret J C, Németh K (2012). Special issue on volcano geomorphology ‘Landforms, processes and hazards’. Introduction. Geomorphology, 136(1): 1–5

Wang Y, Chen H Z (2005). Tectonic controls on the Pleistocene–Holocene WuDalinuoeranchi volcanic field (northeastern China). J Asian Earth Sci, 24(4): 419–431

Wei H Q, Bai Z D, Zhang B L, Hu J C, Shi L B, Xu D B, Sun Q, Fan Q C (2003). Nomenclature of the Holocene volcanic systems and research on the textural parameters of the scoria cones in northern Hainan island. Seismology and Geology, 25(Suppl): 21–30 (in Chinese)

Wood C A (1980). Morphometric evolution of cinder cones. J Volcanol Geotherm Res, 7(3–4): 387–413

Wu Y (1995). Landscape development and characteristics of Inner Mongolia. Yinshan Academic Journal (NATU. SCI.), 13(1): 32–35 (in Chinese)

Yang J J (1988). Study on the petrology of Cenozoic basalt in the XiMeng, Inner Mongolia. Acta Petrologica Sinica, 2: 13–31 (in Chinese)

Yang R X, Bai Z D, Tan Q W, Wu Z L, Wang Y (2012). Study on the geology of Gezishan volcano in Xilinhot, Inner Mongolia. Acta Petrologica Sinica, 28(4): 1181–1188 (in Chinese)